ACS APPLIED MATERIALS & INTERFACES

Research Article

www.acsami.org

Antimicrobial Electrospun Biopolymer Nanofiber Mats Functionalized with Graphene Oxide–Silver Nanocomposites

Andreia F. de Faria,[†] François Perreault,[†] Evyatar Shaulsky,[†] Laura H. Arias Chavez,[‡] and Menachem Elimelech*,[†]

[†]Department of Chemical and Environmental Engineering, Yale University, New Haven, Connecticut 06520-8286, United States

[‡]Department of Chemical Engineering, Tennessee Technological University, Cookeville, Tennessee 38505, United States

Supporting Information

ABSTRACT: Functionalization of electrospun mats with antimicrobial nanomaterials is an attractive strategy to develop polymer coating materials to prevent bacterial colonization on surfaces. In this study we demonstrated a feasible approach to produce antimicrobial electrospun mats through a postfabrication binding of graphene-based nanocomposites to the nanofibers' surface. A mixture of poly(lactide-*co*-glycolide) (PLGA) and chitosan was electrospun to yield cylindrical and narrow-diameter (356 nm) polymeric fibers. To achieve a robust antimicrobial property, the PLGA–chitosan mats were functionalized with graphene oxide decorated with silver nanoparticles (GO–Ag) via a chemical reaction between the carboxyl groups of graphene and the primary amine functional groups on the PLGA–chitosan fibers using 3-(dimethylamino)propyl-*N*′-ethylcarbodiimide hydrochloride and *N*-hydroxysuccinimide as cross-linking agents. The attachment of GO–Ag sheets to the surface of PLGA–chitosan fibers was successfully revealed by scanning and transmission electron images. Upon direct contact with bacterial cells, the PLGA–chitosan mats functionalized with GO–Ag nanocomposites were able to effectively inactivate both Gram-negative (*Escherichia coli* and *Pseudomonas aeruginosa*) and Gram-positive (*Staphylococcus aureus*) bacteria. Our results suggest that covalent binding of GO–Ag nanocomposites to the surface of PLGA–chitosan mats opens up new opportunities for the production of cost-effective, scalable, and biodegradable coating materials with the ability to hinder microbial proliferation on solid surfaces.

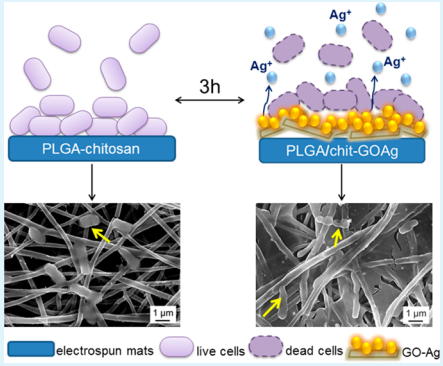

KEYWORDS: *graphene oxide, silver nanoparticles, nanocomposites, electrospun fibers, antimicrobial properties*

INTRODUCTION

The colonization of surfaces by microbes and subsequent biofilm development have attracted much attention due to their ability to cause corrosion on metallic surfaces, decrease performance of filtration membranes, and spread infectious diseases.[1−3] Biofilm formation has also been linked to the appearance of antibiotic-resistant bacteria.[4] The increased resistance of biofilm-associated microorganisms to antimicrobial compounds is a major concern, especially in hospital facilities. For instance, in the United States, the annual expense to treat hospital-acquired nosocomial infections can reach US$ 5 billion.[5] Microbial contamination of medical devices alone is the cause of 60−70% of such infections.[6] Hence, preventing microorganisms from adhering to and developing on solid surfaces is a technical challenge that might be overcome through the development of coating materials with antimicrobial properties.

The fabrication of polymeric nanofibers through electrospinning is a scalable and cost-effective method to obtain coating materials for a wide range of applications. Electrospinning can produce flexible nonwoven fibers with micro- or nanoscale diameters from either synthetic or natural polymers.[7,8] Electrospun fibers display many desirable characteristics such as high surface area and porosity, absorbability of liquids, semipermeability for vapors and gases, and enhanced capability for chemical functionalization.[8,9] These promising features render electrospun mats a suitable platform to fabricate new hybrid materials able to mitigate microbial adhesion and growth.

A number of antimicrobial compounds or antibiotics can be incorporated in electrospun mats to prevent microbial contamination and infection.[10,11] However, since the indiscriminate use of conventional antibiotics has been associated with the development of antibiotic-resistant bacteria, the application of nanomaterials as an alternative class of antimicrobial agents has gained popularity. In addition to single-walled carbon nanotubes,[7] zinc oxide,[12] and silver nanoparticles (AgNPs),[13] graphene-based materials have emerged as attractive nanomaterials for microbial inactivation.[14−16]

Received: February 20, 2015
Accepted: May 17, 2015
Published: May 17, 2015

DOI: 10.1021/acsami.5b01639
ACS Appl. Mater. Interfaces 2015, 7, 12751−12759

Graphene is composed of sp^2-hybridized carbon atoms linked to each other through a honeycomb lattice structure to form a one-atom-thick sheet.[17] Among the several methods used to prepare single-layered graphene sheets, the production of graphene oxide (GO) via chemical exfoliation of graphite is one of the most scalable and reproducible strategies. For this reason, GO has been considered the most common derivative form of graphene. The oxygen functional groups (hydroxyl, epoxy, and carboxyl groups) distributed on the basal plane and over the edges of the aromatic lattice of GO confer high stability against aggregation in aqueous solutions and are likely responsible for the high reactivity of GO sheets.[18,19] Because of its high surface area and amenability to chemical modification, GO has risen as a promising carbon nanomaterial for biological applications.[18]

Nanocomposites of GO sheets with AgNPs (GO−Ag) have shown strong antibacterial activity to Gram-positive and Gram-negative bacteria.[15,20,21] The oxygenated groups on GO can serve as nucleation sites for growth and anchoring of AgNPs. In comparison to pristine AgNPs, GO−Ag nanocomposites benefit from properties of both components in the system.[22,23] The antimicrobial activity of GO−Ag nanocomposites is attributed to the presence of AgNPs, whereas GO provides a high surface area for cellular interaction and deposition. Additionally, the high concentration of oxygenated groups confers to GO−Ag sheets the versatility to bind to solid surfaces via covalent and noncovalent interactions, thus providing multiple opportunities to develop multifunctional materials with antimicrobial activity.[16,19]

The production of antimicrobial coatings from the surface functionalization of electrospun mats with nanomaterials can be carried out using layer-by-layer assembly,[24] electrostatic interactions between oppositely charged materials,[25] and chemical reactions with functional groups.[26] All three methods are based on postfabrication functionalization of electrospun mats. In comparison to the conventional blending process, surface modification via postfabrication possesses several advantages, such as reduced cost due to use of fewer nanomaterials to achieve equivalent properties, scalability of the process, and ability to fine-tune the surface properties.[27]

In this study, we report the fabrication and functionalization of electrospun mats with GO and GO−Ag nanocomposites. The nanofibers were fabricated by electrospinning a blend of poly(lactide-*co*-glycolide) (PLGA) and the natural polymer chitosan. GO−Ag nanocomposites were prepared through an in situ method using sodium borohydrate as a reducing agent. Primary amine functional groups on PLGA−chitosan mats were used as anchor sites for binding GO and GO−Ag sheets to the nanofibers' surface. The fabricated GO−Ag functionalized nanofibers demonstrated a remarkable antimicrobial activity upon contact with Gram-positive and Gram-negative bacteria. Our results highlight the potential use of the GO−Ag modified nanofibers as an effective biocidal coating material for a variety of biomedical and environmental applications.

MATERIALS AND METHODS

Materials and Chemicals. Potassium persulfate ($K_2S_2O_8$, 99.0%), phosphorus pentoxide (P_2O_5, 98.0%), potassium permanganate ($KMnO_4$, 99.0%), hydrochloric acid (HCl, 37.0%), silver nitrate ($AgNO_3$, 99%), sodium borohydride ($NaBH_4$, 99%), MES monohydrate (99%), *N*-(3-(dimethylamino)propyl)-*N*′-ethylcarbodiimide hydrochloride (EDC, 98%), *N*-hydroxysuccinimide (NHS, 98%), trifluoracetic acid (TFA, 99%), poly(lactic-*co*-glycolic acid) (PLGA, 85:15 PLA/PGA, MW: 190 000−240 000 Da), chitosan (MW: 140 000−220 000), ethanol anhydrous (99.5%), glutaraldehyde solution (50%), paraformaldehyde (95%), sodium phosphate dibasic heptahydrate (>99%), and monobasic potassium phosphate (99%) were obtained from Sigma-Aldrich (St. Louis, MO). The graphite sample (SP-1, grade 325 meshes) was purchased from Bay Carbon (Bay City, MI) and used as received. Sulfuric acid (H_2SO_4, 95.0%) and hydrogen peroxide (H_2O_2, 30.0%) were obtained from J. T. Baker (Phillipsburg, NJ). 1,1,2-Trichloro-1,2,2-trifluoroethane (Freon, 99%) was purchased from America Refrigerants (Sarasota, FL). Deionized (DI) water was supplied by a Millipore System (Millipore Co., Billerica, MA).

Synthesis and Characterization of GO and GO−Ag Nanocomposites. Single-layer graphene oxide (GO) sheets were produced by the modified Hummers method[28] as previously described.[29] Briefly, the SP-1 graphite (1.0 g) was submitted to a preoxidation treatment where the graphite powder was placed into concentrated sulfuric acid (5 mL) previously heated at 80 °C. Then, $K_2S_2O_8$ (1.0 g) and P_2O_5 (1.0 g) were added to the graphite suspension and the reaction was carried out at 80 °C for 4.5 h. Shortly after, the graphite solution was placed into 160 mL of DI water and the suspension was left to rest overnight. The solution was then vacuum filtered using PTFE (polytetrafluoroethylene) membranes (0.45 μm, Millipore) and washed with DI water to remove excess acid and reactants. The black solid (preoxidized) was transferred to a Petri dish and left to dry overnight at room temperature.

In the second step, the preoxidized graphite was placed into H_2SO_4 (40 mL), and concentrated $KMnO_4$ (5.0 g) was slowly added to the graphite suspension, using an ice bath to prevent the temperature from rising above 10 °C. Following the $KMnO_4$ addition, the mixture reacted at 35 °C for 2.5 h. After the oxidation reaction, DI water (77.0 mL) was introduced into the suspension and the temperature was controlled so as not to exceed 50 °C. Next, the mixture was left to react for an additional 2 h at room temperature. The solution was then transferred to 240 mL of DI water; 4.2 mL of H_2O_2 (30%) was then added to the dispersion, resulting in the formation of a bright yellow color. The solution was allowed to rest for 2 days. The precipitate was then recovered by centrifugation (12 000*g* for 30 min) and washed with HCl (10% v/v) and DI water to remove chemical residues. Finally, the resulting material was resuspended in DI water and additionally purified by dialysis (3500 Da membranes, Spectrum Laboratories, Inc., CA) for 3−4 days. The resulting dark brown graphite oxide suspension was dried by lyophilization and stored in a sealed Falcon tube.

The GO−Ag nanocomposite was prepared by using silver nitrate ($AgNO_3$) and sodium borohydride ($NaBH_4$) as a salt precursor and reducing agent, respectively. To prepare a colloidal suspension, GO (12.5 mg) was dispersed in DI water (43.75 mL) followed by 30 min of sonication in an ultrasonic bath (Aquasonic Model 150T) and an additional 10 min in a probe sonicator (Misonix model 3000, Farmingdale, NY). $AgNO_3$ (8.65 mg) was dissolved in 5 mL of DI water and then added to the GO suspension. The mixture was subjected to bath sonication for an additional 30 min to provide effective contact between the Ag^+ ions and the oxygenated functional groups on the GO surface. The flasks were then kept in an ice bath for 30 min before the addition of $NaBH_4$. After the suspension was cooled, 2.25 mL of a $NaBH_4$ solution (1 mM) was added dropwise. The reaction was maintained at room temperature for 12 h. The solution slowly turned dark brown, indicating nanocomposite formation. The GO−Ag nanocomposite was purified by dialysis (3500 Da membranes, Spectrum Laboratories, Inc., CA) for 3 h, frozen in liquid nitrogen, and freeze-dried by lyophilization.

The presence of AgNPs in the GO−Ag nanocomposite was confirmed by UV−vis spectroscopy through the detection of the plasmon absorption band. The UV−visible spectra were recorded from 200 to 800 nm using a Hewlett-Packard 8453 spectrophotometer. Thermogravimetric analysis (TGA) was carried out using a Setaram Setsys 1750 TG/DTA. The analyses were obtained using 10 mg of sample, and the temperature was increased from 100 to 800 °C at a rate of 5 °C/min under synthetic air. Information regarding the

DOI: 10.1021/acsami.5b01639
ACS Appl. Mater. Interfaces 2015, 7, 12751−12759

morphological properties of the GO and GO−Ag nanocomposite was obtained through transmission electron microscopy (TEM). The samples were 20 times diluted in DI water, bath sonicated for 10 min, and 5 μL of this dispersion was drop-cast onto copper TEM grids (Formvar/carbon, 200 meshes, Ted Pella, Inc., Redding, CA). The scans were taken in an FEI Tecnai Osiris microscope, operating at an acceleration voltage of 200 kV. Atomic force microscopy (AFM) images of GO were taken in a tapping mode (Bruker Multimode, Digital Instruments, Plainview, NY) using a Tap300Al-G cantilever (BudgetSensors). For the AFM measurements, 3 μL of a graphene oxide suspension (50 μg/mL) were drop-cast on a 1 cm^2 mica wafer previously cleaned under UV-ozone treatment for 20 min (UV/Ozone ProCleaner, BioForce Nanosciences, Ames, IA). The presence of functional groups on the GO sample was investigated by X-ray photoelectron spectroscopy. The spectra were acquired by using a PHI 5000 VersaProbe Instrument (Physical Electronics, Chanhassen, MN), operating with a monochromatic Al kα X-ray source ($h\nu$ = 1486 eV).

Fabrication of PLGA and PLGA−Chitosan Nanofibers. PLGA (0.35 g) was added to 5.0 mL of trifluoracetic acid (TFA) and the polymer suspension was incubated at 30 °C and mixed overnight using a tube rotator (Elmeco Arma-A1, Rockville, MD). The blend PLGA−chitosan was prepared by adding 0.035 g of chitosan into the previously prepared PLGA solution. The final ratio of chitosan in the blend was 10 wt % (relative to PLGA weight). After incubation, the PLGA and PLGA−chitosan solutions were loaded into a 5-mL plastic syringe fitted with a metal 21-gauge needle (Becton, Dickinson & Co.). The syringe was placed horizontally on the syringe pump (Harvard Apparatus, Plymouth Meeting, PA), and a voltage supply (Gamma High Voltage Research Inc., Ormond Beach, FL) was attached to the needle tip and to the collector plate via alligator clips. The needle-to-collector distance was 11 cm, and a rectangular glass plate (Thermo Scientific, 25 × 75 mm, 1.0 mm thick) was used to collect the fibers. The flow rate and the applied voltage were 0.4 mL/h and 14.5 kV, respectively. Electrospinning was conducted under controlled conditions of temperature (30.0 ± 0.5 °C) and relative humidity (9−13%).

Surface Functionalization of PLGA−Chitosan Nanofiber Mats with GO and GO−Ag. The surface of the PLGA−chitosan electrospun mats was chemically modified with GO and GO−Ag nanocomposite using the coupling agents EDC and NHS. The methodology applied to functionalize the fibers with GO and GO−Ag was adapted from our previous publications.[16,30] The modified fibers were denoted as PLGA/chit−GO and PLGA/chit−GOAg.

The functionalization process comprised two steps. The first step consisted of activation of the carboxylate functional groups on the GO or GO−Ag sheets in the presence of EDC and NHS. For the first step, 25 mL of the GO or GO−Ag dispersions (250 μg/mL) (prepared as described earlier in the paper in Synthesis and Characterization of GO and GO−Ag Nanocomposites) was mixed with 20 mL of MES buffer (pH 6.1). Then, EDC (8.65 mg) and NHS (19.4 mg) were dissolved in 5 mL of MES pH at 6.1 and introduced into the GO or GO−Ag dispersion. EDC and NHS were allowed to react with the graphene materials for 30 min, and, during this exposure, the carboxylic groups on GO or GO−Ag nanocomposite were converted to an intermediate semistable reactive ester. The addition of EDC and NHS lowered the pH of the solution to 5.8. After activation, the pH of the GO or GO−Ag suspension was raised to 7.2 using a sodium hydroxide solution (1 M). The final concentrations of GO and GO−Ag, EDC, and NHS in the reaction media were 125 μg/mL, 1.5 mM, and 2.5 mM, respectively.

In the second step, 4 mL of the activated GO or GO−Ag suspension was added to a 3 cm^2 PLGA−chitosan fiber coupon (attached to a glass support), and the system was gently stirred at room temperature for 3 h. In this phase, the activated ester on the GO or GO−Ag sheets reacted with the amine functional groups on the PLGA−chitosan electrospun mats, thus forming amide bonds that attached the nanomaterials to the fiber surface. After reaction, the GO or GO−Ag suspension was discarded and the fibers were rinsed with DI water to remove the excess unbound graphene materials. The modified fibers were dried at room temperature for 24 h.

Characterization of As-Spun and Functionalized Nanofiber Mats. The presence of chitosan on the PLGA−chitosan fiber was investigated by Fourier transform infrared spectroscopy (FTIR). The spectra were recorded from 500 to 400 cm^{-1} using a Thermo Nicolet 6700 spectrometer. The fibers' morphology was examined using a Hitachi scanning electron microscope (SEM) SU-70. A Denton (model Desk V) sputtering machine was applied to coat the sample with a 10-nm layer of chromium. Fiber diameter distribution was determined using ImageJ software (National Institutes of Health, Bethesda, MD) by randomly measuring the diameter of 100 fibers from different SEM images of the same sample. The presence of GO and GO−Ag nanocomposite on the PLGA/chit−GO and PLGA/chit−GOAg fibers was also verified by SEM. The binding of GO and GO−Ag to the fibers' surface was also confirmed by Raman spectroscopy. The Raman spectra were acquired utilizing a 532-nm laser excitation on a Horiba Jobin Yvon HR-800 Raman spectrometer. The hydrophilicity of the fibers' surface was evaluated by measuring the water contact angle using a Theta Lite Optical Tensiometer TL100 (Attension, Espoo, Finland). Contact angles were measured at four randomly selected locations on each sample (PLGA, PLGA−chitosan, PLGA/chit−GO, PLGA/chit−GOAg).

The morphology of the fiber mats modified with GO−Ag nanocomposite was also investigated by transmission electron microscopy (TEM). To obtain the TEM images of the surface, the lower layers of fibers in the PLGA/chit-GOAg mats were peeled off from below using a commercial scotch tape (Shipping Package Tape, 3 M Scotch). This procedure was performed until a very thin layer was isolated. The mat surfaces were then dropped on copper grids and examined in an FEI Tecnai Osiris microscope, operating at an acceleration voltage of 200 kV. To quantify the silver release, PLGA/chit-GOAg coupons (∼3 cm^2) were placed in small Petri dishes and 5 mL of DI water was introduced. During the first 12 h, the solution was collected every 2 h, and the Petri dishes containing the fiber mats were refilled with an additional 5 mL of DI water (pH ∼ 6.0) each time, under aerobic conditions. The solution containing the silver ions was then stored in scintillation vials at 4 °C for further analysis. After 12 h, the washing procedure was performed every 24 h. Subsequently, the samples were acidified with concentrated HNO_3 and the silver concentration was quantified by an inductively coupled plasma mass spectrometer (ICP-MS, PerkinElmer, Waltham, MA).

Evaluation of Antibacterial Activity of GO-Ag Mats. *Escherichia coli*, *Pseudomonas aeruginosa*, and *Staphylococcus aureus* were used as model microorganisms. *E. coli* (ATCC BW26437) was received from Yale Coli Genetic Stock Center (New Haven, CT). *P. aeruginosa* (ATCC 27853) was obtained from the American Type Culture Collection, and *S. aureus* 8325 was kindly provided by Dr. Naomi Balaban. The bacterial strains were cultured in Luria−Bertani broth (LB) and incubated at 37 °C overnight. After incubation, the bacterial cells were cultivated to log phase by diluting the overnight culture (1 mL) into a fresh LB medium (9 mL) and growing for 2 h until reaching an optical density of 1.0 at 600 nm ($OD_{600\ nm}$). The log-phase growth time was determined by a growth curve. The cultures were then washed three times to remove the excess macromolecules and other medium constituents, and resuspended in a sterile isotonic solution (PBS buffer, 0.01 M, pH 6.8). The cultures were diluted in PBS to reach an $OD_{600\ nm}$ of 0.1, which corresponds to a concentration of ∼10^7 CFU mL^{-1} for all three strains tested. Cell density was determined by plate counting.

The antibacterial activity of the GO and GOAg functionalized nanofibers was assessed using plate counting. To study their toxicity to *E. coli*, *P. aeruginosa*, and *S. aureus*, the electrospun mats (PLGA, PLGA−chitosan, PLGA/chit-GO, and PLGA/chit-GOAg) were placed at the bottom of plastic Petri dishes, and an aliquot of the bacterial suspension (4 mL, 10^7 cells/mL) was added. The fibers and the bacteria suspension were kept in contact for 3 h at room temperature. The excess bacterial suspension was then discarded and the fiber coupons were rinsed with PBS buffer (pH 6.8) to remove the unattached bacteria. The fiber coupons were transferred to 50-mL Falcon tubes containing 20 mL of a sterile PBS buffer (pH 6.8) and bath sonicated for 10 min to remove the attached bacteria cells from

DOI: 10.1021/acsami.5b01639
ACS Appl. Mater. Interfaces 2015, 7, 12751−12759

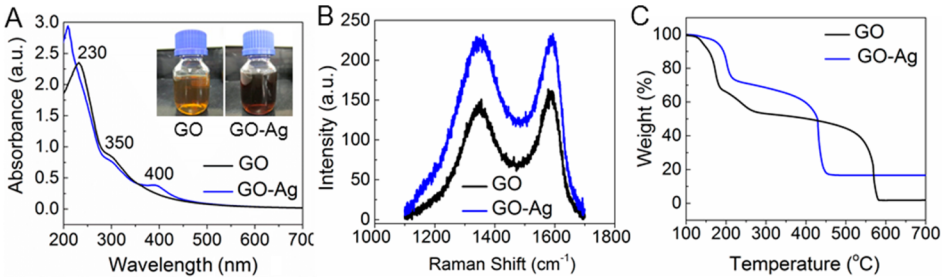

Figure 1. (A) UV−vis spectra of GO and GO−Ag nanocomposite dispersion (75 μg mL^{-1}) evidencing the plasmonic band at 400 nm, characteristic of silver nanoparticles (AgNPs) formation. The photographs illustrate the color of the GO suspension before and after functionalization with AgNPs. (B) Raman spectra displaying the typical presence of "D" and "G" bands for GO and GO−Ag. (C) Thermogravimetric analysis (TGA) of GO and GO−Ag, demonstrating their weight loss profiles. The silver content of the GO−Ag is about 20 wt %.

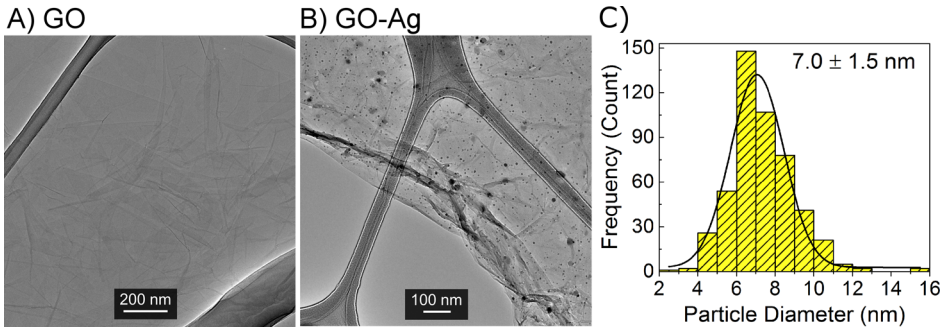

Figure 2. TEM micrographs of (A) GO and (B) GO−Ag sheets, and (C) size distribution of AgNPs formed on GO sheets. More than 400 nanoparticle diameters were randomly selected from TEM images and analyzed using ImageJ software.

the fibers' surface. The supernatant was sequentially diluted, spread on LB agar plates, and incubated overnight at 37 °C. After incubation, the grown colonies were counted and the number of bacteria attached to the fibers' surface was expressed as CFU mL^{-1}.

After the bacteria were in contact with the electrospun mats, the morphology of the attached cells was observed through SEM. The fiber coupons were rinsed with sterile PBS pH 6.8 and fixed by using a Karnovsky's solution (2% paraformaldehyde and 2.5% glutaraldehyde diluted in 0.2 M Sorenson's buffer, pH 7.2) for 3 h. The attached cells were consecutively dehydrated by immersing the fiber coupons in water−ethanol (50:50, 30:70, 20:80, 10:90, and 100% ethanol) and ethanol−freon solutions (50:50, 25:75, and 100% freon) for 10 min each. After the sequential dehydration steps, the fiber coupons were dried overnight in a desiccator at room temperature. The samples were then sputter-coated with 10 nm of chromium (Denton Vacuum, Desk V), and the bacteria cells were imaged by SEM (Hitachi SU-70) operating at an acceleration voltage of 5−10 kV.

RESULTS AND DISCUSSION

Physicochemical Properties of GO and GO−Ag. Preparation of GO was confirmed by scanning electron microscopy (SEM), as shown in Supporting Information (SI) Figure S1A. The size distribution was obtained by measuring the area of GO sheets in multiple SEM micrographs, revealing an average size of 0.36 ± 0.37 μm^2 (SI Figure S1B). Atomic force microscopy (AFM) imaging showed GO sheets around 1.0 nm thick, which suggests the presence of single-layer exfoliated sheets (SI Figure S2A). The presence of functional groups on GO sheets was analyzed by X-ray photoelectron spectroscopy (XPS). The deconvoluted spectra for C 1s XPS (SI Figure S2B) display peaks assigned to C−C bonding of sp^2 (284.3 eV) and C−C bonds of sp^3 carbon components (285.3 eV), C—O single bonds of epoxy and hydroxyl groups (C—O; 286.4 eV), and C═O double bonds of carboxyl moieties (C═O, 288−289 eV).[22,29] The C/O ratio of GO sheets was around 1.9−2.0, indicating the abundance of oxygenated groups. The O 1s XPS spectra for the GO sample are also seen in SI Figure S2B. The O 1s XPS spectra show three deconvoluted peaks associated with adsorbed oxygen components (531.1 eV), oxygen double bonds of carbonyl and carboxyl groups (O═C, O—C═O; 532.3 eV), and single oxygen bonds of ether and hydroxyl groups (C—O—C, C—O; 533.5 eV).

During the synthesis of GO−Ag, the nanomaterial suspension turned dark brown as silver ions were reduced to AgNPs on GO sheets (Figure 1A). As also shown in Figure 1A, the UV−vis spectrum of the GO exhibits a characteristic absorption peak at 230 nm that is related to the electronic $\pi-\pi^*$ transitions of C—C aromatic bonds and a shoulder at 305 nm which is assigned to the n−π^* transitions of C═O bonds.[31] The presence of a surface plasmon band at 400 nm in the GO−Ag sample (Figure 1A) is indicative of the AgNP deposition on GO sheets.[20,32]

The functionalization of GO with AgNPs was also investigated by Raman spectroscopy. The Raman spectrum of GO shows the presence of the characteristic D band at 1320 cm^{-1} and G band at 1570 cm^{-1},[21,33] as shown in Figure 1B. After incorporation of AgNPs on the GO surface, the intensities of both D and G bands were increased. The increase in the Raman scattering can be attributed to surface-enhanced Raman scattering (SERS), as previously described.[34,35] Furthermore, the intensity ratio between D and G bands (I_D/I_G) was found to increase from 0.89 to 0.99 after functionalization of GO sheets with AgNPs. This increased I_D/I_G ratio indicates a reduction in the sp^2 domain as a consequence of the attachment of AgNPs on the GO surface. Similar results were also reported by previous studies regarding the decoration of GO sheets with AgNPs.[15,32,35]

DOI: 10.1021/acsami.5b01639
ACS Appl. Mater. Interfaces 2015, 7, 12751−12759

Thermogravimetric analysis of GO and GO−Ag was also performed (Figure 1C). The weight losses observed up to 250 °C are associated with the decomposition of the oxygenated functional groups on GO surface, whereas the second and major weight loss around 500 and 600 °C is attributed to the thermal decomposition of the graphitic layer.[36] A significant reduction in the decomposition temperatures for GO−Ag nanocomposites was observed. Specifically, the second weight loss for the GO−Ag (at 400 °C) took place at approximately 200 °C lower than that observed for GO (at 600 °C). This phenomenon is likely associated with the presence of AgNPs, which may act as catalysts, thus reducing the temperature of decomposition for GO−Ag nanocomposites.[15] Lastly, the amount of residue above 700 °C was related to the silver content in the GO−Ag nanocomposite. According to the thermogravimetric curve, the relative percentage of silver in the GO−Ag nanocomposite is about 18 wt % (Figure 1C).

The morphological characteristics of GO and GO−Ag nanocomposite were evaluated by high-resolution transmission electron microscopy (TEM) (Figure 2). On the holey carbon TEM grids, GO exhibited a natural tendency to unfold and present a flake-like and wrinkled morphology (Figure 2A). TEM micrographs confirmed the functionalization of GO sheets with AgNPs (Figure 2B). Sphere-like AgNPs were well distributed throughout the graphene sheet surface with an average size of 7.0 ± 1.5 nm, and no particles were found to be detached from the GO surface (Figure 2C). The nucleation of the AgNPs may be attributed to the interaction of Ag^+ ions with the negatively charged carboxylic acid groups or even the epoxy and hydroxyl groups on GO sheets, which provide sites for anchoring and growth of the nanoparticles.[22,37,38]

Structure of the As-Spun Nanofiber Mats. Poly(lactic-*co*-glycolic acid) (PLGA) was chosen as a precursor polymer because of its biocompatibility, biodegradability, and outstanding mechanical properties. PLGA is an FDA-approved polymer that has been used for biomedical applications, including the production of surgical sutures and clips, controlled-release implants, and drug delivery systems.[8,39,40] SEM micrographs (Figure 3A) show that the as-spun PLGA electrospun mats comprise cylindrical and ribbon-like nanofibers. Although the as-spun PLGA mats were highly heterogeneous in terms of morphology, the presence of beads or branched structures was not observed (Figure 3A). The as-spun PLGA mats showed an average fiber diameter of 885 ± 485 nm (Figure 3B).

To incorporate amine functional groups to the PLGA fibers, chitosan, a natural polysaccharide derivative from chitin, was incorporated in the PLGA solution. SEM micrographs of the PLGA−chitosan mats revealed the presence of smooth and cylindrical nanofibers (Figure 3B). In comparison to the pure PLGA mats, the morphology of the PLGA−chitosan fibers was found to be more homogeneous; also, ribbon-like structures were no longer observed in the hybrid material (Figure 3C).

The PLGA−chitosan electrospun mats showed an average fiber diameter of 351 ± 81 nm (Figure 3D), which is significantly lower than that of the as-spun PLGA fibers. A similar trend has been observed for poly(vinyl alcohol) (PVA) nanofibers blended with chitosan.[41] A mixture of PLGA with different concentrations of collagen also led to fibers with smaller diameter.[42] This effect has been attributed to the ionization of chitosan under acidic conditions. The presence of chitosan can provide an increased charge density on the surface of the jet, which leads to enhanced conductivity and self-repulsion of the stretching solution under the electrical field.[41,43] It is worthy of note that the morphology of electrospun mats can also be influenced by the viscosity of the precursor solution and polymer concentration.[8,9,44]

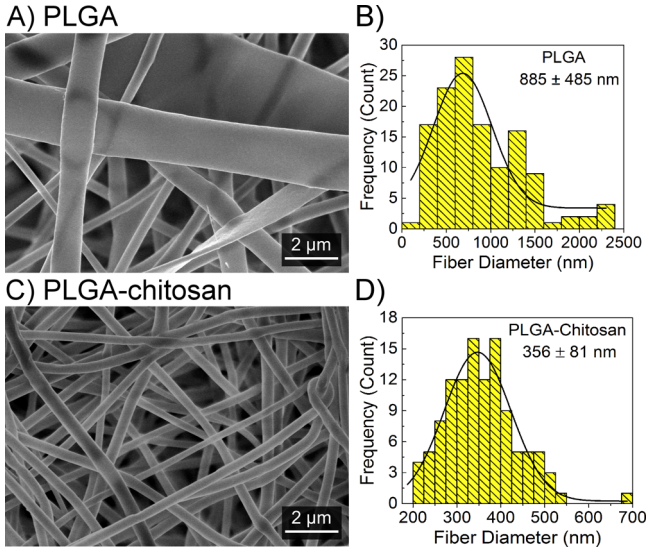

Figure 3. SEM micrographs displaying (A) as-spun PLGA mats and (C) PLGA−chitosan mats originated from the blending of PLGA and chitosan. At least 100 randomly selected fibers in multiple micrographs were measured in ImageJ to obtain the corresponding diameter distribution for each composition displayed in B and D.

The chemical composition of as-spun PLGA and PLGA−chitosan fiber mats was investigated by FT−IR spectroscopy (SI Figure S3). The vibrational modes at around 2990 and 2930 cm^{-1} are attributed to the symmetric and asymmetric C—H stretch of alkanes (CH_2) on PLGA (SI Figure S3A). The strong vibrational mode at 1749 cm^{-1} is related to the C═O stretch of ester carbonyl groups. In addition, the characteristic peak at 1456 cm^{-1} is assigned to the C—H vibration mode of methyl (CH_3) groups. Peaks below 1400 cm^{-1} in the PLGA spectrum can be mostly associated with C—O bonds. More precisely, the peaks at 1128 and 1087 cm^{-1} are, respectively, ascribed to the C—O stretch of ester and ether groups of PLGA.[43,45,46] Note that the FT−IR spectrum for PLGA−chitosan is very similar to that of the as-spun PLGA. However, the PLGA−chitosan mats exhibited two clear vibrational modes at 1680 and 1550 cm^{-1} that were not observed in the as-spun PLGA spectrum (SI Figure S3B). These vibrational modes at 1680 and 1550 cm^{-1} correspond to the C═O stretch and N—H bending of amide I from the acetylated units of chitosan, respectively.[47] Therefore, a certain number of amine groups is modified by acetyl groups (a single methyl bound to a carbonyl group, CH_3—HC═O), resulting in the formation of amide functional groups on the chemical structure of chitosan.[43,46] Even though the N—H stretch mode for primary amine groups was not observed in the FT−IR spectrum, the vibrational modes at 1680 and 1550 cm^{-1} clearly confirm the presence of chitosan on the PLGA−chitosan mats.

Characteristics of Nanofiber Mats Functionalized with GO and GO−Ag. The surface modification procedure is based on the formation of an amide bond through the reaction between the carboxyl groups of GO and the primary amine groups on PLGA−chitosan fibers.[16,19,30] Figure 4 illustrates the covalent binding of GO or GO−Ag nanocomposite to the PLGA−chitosan surface.

DOI: 10.1021/acsami.5b01639
ACS Appl. Mater. Interfaces 2015, 7, 12751−12759

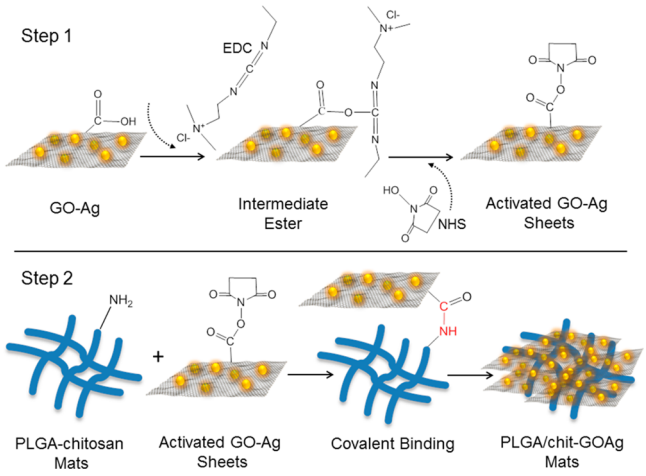

Figure 4. Schematic diagram showing the protocol for covalent binding of GO−Ag nanocomposite to the PLGA−chitosan nanofibers surface. Step1: the native carboxylic groups on GO sheets react with EDC and NHS to form an intermediate activated ester at pH 5.0 (MES buffer). Step 2: the native free amine groups present in the PLGA−chitosan nanofibers react with the intermediate ester, leading to the formation of a stable amide bond which covalently links the GO-based materials with the surface of the electrospun mats.

SEM micrographs for PLGA/chit-GO (Figure 5A and C) and PLGA/chit-GOAg (Figure 5B and D) successfully revealed

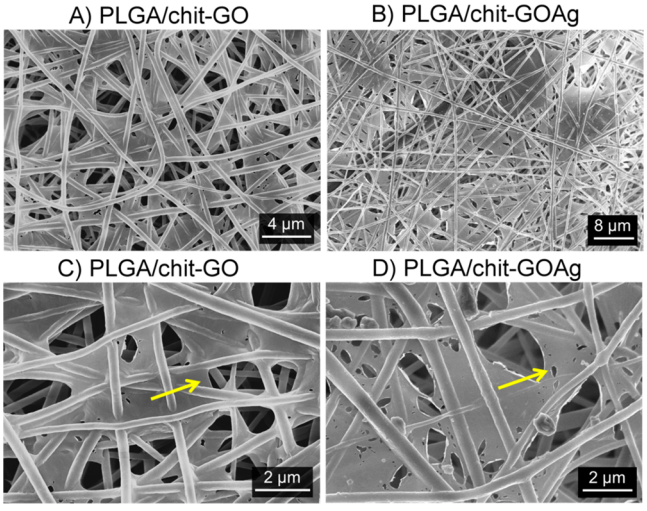

Figure 5. SEM micrographs showing the surface of PLGA−chitosan mats modified with GO sheets (A, C) and the GO−Ag nanocomposite (B, D). Yellow arrows indicate the GO and GO−Ag sheets distributed across the fiber mat surface.

the attachment of GO and GO−Ag sheets on the surface of the fiber mats. As indicated by the yellow arrows in Figure 5, GO and GO−Ag nanocomposites were homogeneously distributed across the top surface of the fibers. However, except for the presence of small bright dots on the PLGA/chit-GOAg mats, no significant differences between PLGA/chit-GO and PLGA/chit-GOAg mats were observed from the SEM micrographs. In fact, because the AgNPs anchored to the GO sheets were very small (~7 nm, Figure 2C), they could not be visualized from the SEM micrographs (Figures 5B and D).

To identify the presence of GO−Ag sheets, PLGA/chit-GOAg fiber mats were analyzed by TEM (Figure 6). The TEM

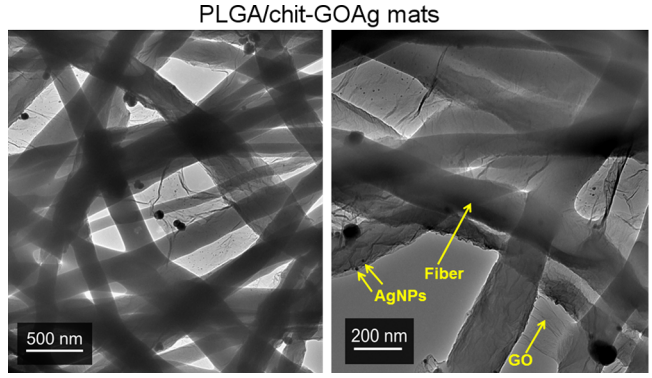

Figure 6. TEM micrographs of PLGA−chitosan mats functionalized with GO−Ag (PLGA/chit-GOAg). The TEM micrographs reveal the GO−Ag sheets decorating the surface of the PLGA−chitosan mats. AgNPs (small black dots), fibers, and GO sheets are identified by the yellow arrows.

micrographs enabled the simultaneous visualization of AgNPs (represented by the black particles attached to GO), GO sheets, and the PLGA−chitosan fibers. All these components are indicated by yellow arrows in Figure 6.

The functionalization of the PLGA−chitosan fibers with GO and GO−Ag nanocomposites was also confirmed by Raman spectroscopy (Figure 7A). For pristine PLGA and PLGA−chitosan electrospun mats, no prominent bands at the range of 1300−1600 cm^{-1} were observed. However, upon modification with GO and GO−Ag, the presence of the characteristic D (1350 cm^{-1}) and G (1580 cm^{-1}) bands became evident in the Raman spectra for PLGA/chit-GO and PLGA/chit-GOAg mats, confirming the attachment of graphene-based materials. As-spun PLGA mats were significantly hydrophobic with a contact angle of 118 ± 2.4°, which is consistent with previous studies on PLGA electrospun fibers (Figure 7B).[43,48] PLGA−chitosan fibers exhibited a slightly lower contact angle (106 ± 1.5°) compared to the pristine PLGA mats due to the hydroxyl (−OH) groups of chitosan that can form hydrogen bonds with water molecules. Similarly, previous studies revealed that the incorporation of chitosan in PLGA nanofibers (ratio 1:9) resulted in a decrease of the contact angle from 116 to 81°.[43] Significant differences in the contact angle were observed for the fibers modified with GO and GO−Ag compared to the nonmodified PLGA−chitosan mats. Grafting of GO and GO−Ag decreased the contact angle of the PLGA−chitosan mats from 106 ± 1.5° to 56 ± 8.4° and 74.5 ± 1.3°, respectively. The improved wettability of the composite nanofibers is attributable to the increased number of oxygen groups on the surface of the PLGA−chitosan mats after functionalization with GO and GO−Ag. This observation is consistent with previous studies that applied contact angle measurements to confirm the binding of oxygenated single-walled carbon nanotubes and GO sheets to the surface of polymeric membranes.[16,30]

Antimicrobial Activity of Functionalized Mats. Figure 8 displays the antibacterial activity of PLGA/chit-GOAg mats after 3 h of contact with *E. coli*, *P. aeruginosa*, and *S. aureus*. The PLGA/chit-GOAg fibers exhibited a bacterial inactivation rate of over 98% for *E. coli* and *P. aeruginosa*, relative to the nonmodified control PLGA−chitosan. However, a lower inactivation rate of 79.4 ± 6.1% was achieved against *S. aureus*. The observed results are related to the differences in the structural morphology of the bacterial cell wall. In comparison to Gram-negative bacteria, the cell wall of Gram-positive

DOI: 10.1021/acsami.5b01639
ACS Appl. Mater. Interfaces 2015, 7, 12751−12759

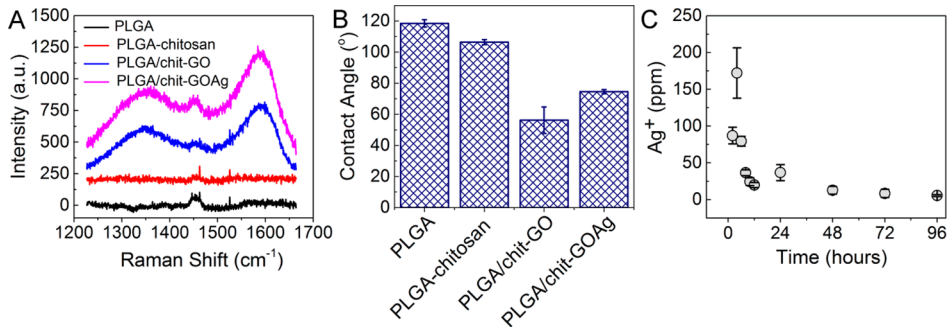

Figure 7. (A) Raman spectra and (B) contact angle measurements of PLGA, PLGA−chitosan, PLGA/chit-GO, and PLGA/chit-GOAg mats. (C) Silver releasing from PLGA−chit−GOAg electrospun mats after sequential washing-steps with 5 mL of DI water. For the first 12 h, the PLGA/chit-GO fiber mats were washed every 2 h. After 24 h, the washing process was performed with a 24-h time interval.

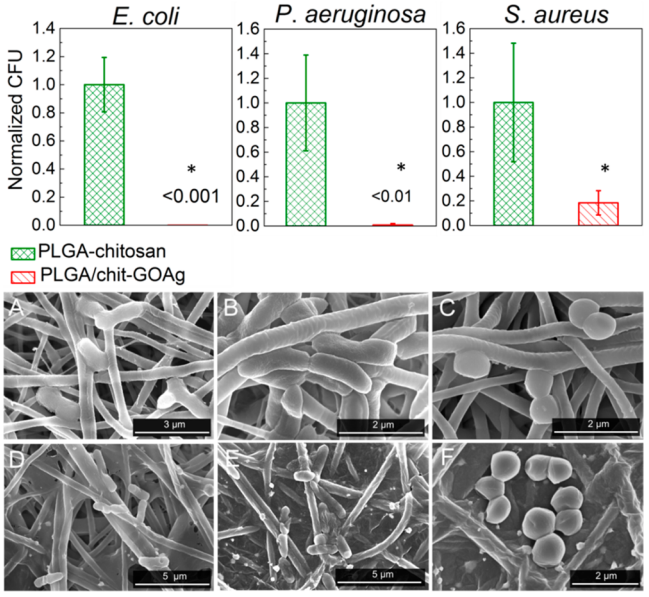

Figure 8. Top: Number of attached viable bacteria cells on PLGA−chitosan (control) and PLGA/chit-GOAg after exposure to Gram-negative (*E. coli* and *P. aeruginosa*) and Gram-positive (*S. aureus*) bacteria. The values were normalized by dividing the number of live attached cells on PLGA/chit-GOAg sample by the number of attached cells on the nonmodified PLGA−chitosan (control). Bottom: SEM micrographs displaying the morphological characteristics of *E. coli* (A, D), *P. aeruginosa* (B, E), and *S. aureus* (C, F) cells after contact with PLGA−chitosan (A, B, and C) and PLGA/chit-GOAg (D, E, and F) modified nanofibers. The statistical significance of the inactivation rates was confirmed through a hypothesis *t*-test. All the inactivation rates of PLGA−chit−GOAg were significantly different from the control PLGA−chitosan with *p*-values of less than 0.05.

bacteria possesses a thicker peptidoglycan layer, which confers to *S. aureus* cells protection against the antibacterial effects of GO−Ag nanocomposites. Our results are in agreement with a previous study on polysulfone mats functionalized with AgNPs, which reported higher inactivation rates for *E. coli* than *S. aureus* cells.[25]

After exposure to the PLGA−chitosan and PLGA/chit-GOAg electrospun mats, the attached cells were examined by SEM, as shown in Figure 8 (bottom). Compared to the PLGA−chitosan mats (Figure 8A, B, C), the attached bacteria cells on PLGA/chit-GOAg (Figure 8D, E, F) lost their morphological integrity upon contact with the GO−Ag nanocomposites. The SEM micrographs show that *E. coli*, *P. aeruginosa*, and *S. aureus* cells became flattened and wrinkled after their exposure to the surface of the PLGA−chit−GOAg nanofibers. These changes in morphological characteristics suggest that the bacterial cells were irreversibly damaged upon contact with the GO−Ag nanocomposites. The SEM micrographs shown in Figure 8 are consistent with previous SEM micrographs obtained for *E. coli* cells inactivated after contact with nanofibers containing AgNPs.[25]

The mechanism of toxicity for GO−Ag nanocomposites is associated with the presence of AgNPs. It is well-known that the toxicity mechanism of AgNPs is related to their surface oxidation and consequent generation of Ag^+ ions,[49] according to the following reaction: $2Ag_{(s)} + (1/2)O_{2(aq)} + 2H^+_{(aq)} \leftrightarrow 2Ag^+_{(aq)} + H_2O_{(l)}$.[50] In addition, the generation of reactive oxygen species (ROS) and destabilization of the cellular membrane by direct contact between the microbial cells and AgNPs have also been hypothesized.[49,51] Previous studies have proposed that the antibacterial activity of GO−Ag nanocomposites results from a synergetic effect between the GO sheets and the AgNPs.[23,52] Once the bacterial cells are deposited on the surface of the PLGA/chit-GOAg mats, they can be inactivated by the AgNPs, while GO sheets provide a large surface area for the effective interaction between microbial cells and the AgNPs anchored to the GO−Ag sheets. Hence, the release of Ag^+ ions combined with the direct interaction between cells and AgNPs on the surface of GO−Ag sheets could explain the bacterial inactivation after exposure to the PLGA−chit−GOAg mats.

Inductively coupled plasma mass spectrometry (ICP−MS) analyses were performed to evaluate the potential release of Ag^+ ions (Figure 7C). The PLGA−chit−GOAg mats showed a maximum Ag^+ ion release at 4 h (172 ± 34 ppm), with the ion release decreasing rapidly in the following washing steps. As the mechanism of toxicity for AgNPs is partially dependent on their capacity to dissolve into Ag^+ ions, the profile of Ag^+ ion release can provide an estimate of the duration of the fibers' biological functionality.

The antibacterial tests were also conducted with PLGA−chitosan fiber modified with GO sheets (without silver). As shown in SI Figure S4, the PLGA/chit-GO electrospun mats did not show significant toxicity against the microorganisms *E. coli*, *P. aeruginosa*, and *S. aureus* ($p > 0.65$). The morphological characteristics of the bacteria cells exposed to the PLGA/chit-GO were also evaluated using SEM. In comparison to the control PLGA−chitosan, no loss of morphological integrity was detected for the attached cells on the PLGA/chit-GO fibers (SI Figure S4A, B, C). The results indicate that direct contact

DOI: 10.1021/acsami.5b01639
ACS Appl. Mater. Interfaces 2015, 7, 12751−12759

between the cells and GO sheets did not cause deleterious effects to the cells. Despite previous studies reporting toxicity to bacteria cells upon direct contact with GO,[16,53−55] we did not observe antibacterial activity for PLGA−chitosan modified with GO sheets. It is worth pointing out that GO toxicity can be influenced by its morphology and physicochemical properties, particularly GO sheet size.[54,56−59] The toxicity can also be affected by the type of model microorganisms as well as by the method used to evaluate the toxicity of the graphene-based materials.[18,54−58,60]

CONCLUSION

We present the functionalization of electrospun nanofiber mats with a graphene−silver nanocomposite to develop flexible coating materials with antimicrobial properties. Graphene oxide (GO) sheets decorated with silver nanoparticles were bound to the surface of PLGA−chitosan nanofibers through a simple postfabrication method utilizing EDC and NHS as cross-linkers. Raman spectroscopy, SEM, and TEM imaging confirmed the successful functionalization of the fibers' surface with the graphene-based nanomaterials. The irreversible binding of GO−Ag sheets to the nanofiber surface imparted remarkable antimicrobial activity to the hybrid mats, leading to an inactivation rate of 99% for Gram-negative (*E. coli* and *P. aeruginosa*) and 76% against Gram-positive (*S. aureus*) bacteria upon direct contact with the microbial cells. Our findings strongly suggest the application of PLGA−chit−GOAg mats as an outstanding antimicrobial coating material to provide antimicrobial activity to surfaces.

ASSOCIATED CONTENT

Supporting Information

Characterization of GO by scanning electron microscopy (SEM) and size distribution of GO sheets (Figure S1); atomic force and X-ray photoelectron microscopy (XPS) of GO sample (Figure S2); Fourier transform infrared spectroscopy (FT−IR) spectra of PGLA and PLGA−chitosan electrospun mats (Figure S3); antibacterial activity of PLGA−chitosan fiber functionalized with GO and SEM micrographs of bacterial cells attached to the same fibers (Figure S4). The Supporting Information is available free of charge on the ACS Publications website at DOI: 10.1021/acsami.5b01639.

AUTHOR INFORMATION

Corresponding Author

*E-mail: menachem.elimelech@yale.edu.

Notes

The authors declare no competing financial interest.

ACKNOWLEDGMENTS

This work was supported by the Program "Science without Borders" through the Brazilian Council of Science and Technology (CNPq Grant 246407/2012-3). A.F.F also thanks Lemann Institute for Brazilian Studies for their financial support. F.P. acknowledges the financial support of the Natural Sciences and Engineering Research Council of Canada postdoctoral fellowship. The authors are grateful to Dr. Siamak Nejati for his support on the XPS analysis. Additionally, the authors acknowledge Yale Institute of Nanoscale and Quantum Engineering (YINQE) and Dr. Michael Rooks for their support on the TEM and SEM analyses.

REFERENCES

(1) Elimelech, M.; Phillip, W. A. The Future of Seawater Desalination: Energy, Technology, and the Environment. *Science* **2011**, *333* (6043), 712−717.
(2) Chmielewski, R. A. N.; Frank, J. F. Biofilm Formation and Control in Food Processing Facilities. *Compr. Rev. Food Sci. Food Saf.* **2003**, *2*, 22−32.
(3) Donlan, R. M. Biofilms: Microbial Life on Surfaces. *Emerging Infect. Dis.* **2002**, *8*, 881−888.
(4) Romero, D.; Kolter, R. Will Biofilm Disassembly Agents Make it to Market? *Cell* **2011**, *19*, 304−306.
(5) Wenzel, R. P. Health Care-Associated Infections: Major Issues in the Early Years of the 21st Century. *Clin. Infect. Dis.* **2007**, *45* (Supplement 1), S85−S88.
(6) Bryers, J. D. Medical Biofilms. *Biotechnol. Bioeng.* **2008**, *100* (1), 1−18.
(7) Schiffman, J. D.; Elimelech, M. Antibacterial Activity of Electrospun Polymer Mats with Incorporated Narrow Diameter Single-Walled Carbon Nanotubes. *ACS Appl. Mater. Interfaces* **2011**, *3* (2), 462−468.
(8) Agarwal, S.; Wendorff, J. H.; Greiner, A. Use of Electrospinning Technique for Biomedical Applications. *Polymer* **2008**, *49* (26), 5603−5621.
(9) Rieger, K. A.; Birch, N. P.; Schiffman, J. D. Designing Electrospun Nanofiber Mats to Promote Wound Healing - A Review. *J. Mater. Chem. B* **2013**, *1* (36), 4531−4541.
(10) Buschle-Diller, G.; Cooper, J.; Xie, Z.; Wu, Y.; Waldrup, J.; Ren, X. Release of Antibiotics from Electrospun Bicomponent Fibers. *Cellulose* **2007**, *14* (6), 553−562.
(11) Kim, K.; Luu, Y. K.; Chang, C.; Fang, D.; Hsiao, B. S.; Chu, B.; Hadjiargyrou, M. Incorporation and Controlled Release of a Hydrophilic Antibiotic using Poly(lactide-co-glycolide)-Based Electrospun Nanofibrous Scaffolds. *J. Controlled Release* **2004**, *98* (1), 47−56.
(12) Anitha, S.; Brabu, B.; Thiruvadigal, D. J.; Gopalakrishnan, C.; Natarajan, T. S. Optical, Bactericidal and Water Repellent Properties of Electrospun Nano-Composite Membranes of Cellulose Acetate and ZnO. *Carbohydr. Polym.* **2012**, *87* (2), 1065−1072.
(13) Rujitanaroj, P.-o.; Pimpha, N.; Supaphol, P. Wound-Dressing Materials with Antibacterial Activity from Electrospun Gelatin Fiber Mats Containing Silver Nanoparticles. *Polymer* **2008**, *49* (21), 4723−4732.
(14) Akhavan, O.; Ghaderi, E.; Esfandiar, A. Wrapping Bacteria by Graphene Nanosheets for Isolation from Environment, Reactivation by Sonication, and Inactivation by Near-Infrared Irradiation. *J. Phys. Chem. B* **2011**, *115* (19), 6279−6288.
(15) de Faria, A. F.; Martinez, D. S. T.; Meira, S. M. M.; de Moraes, A. C. M.; Brandelli, A.; Filho, A. G. S.; Alves, O. L. Anti-Adhesion and Antibacterial Activity of Silver Nanoparticles Supported on Graphene Oxide Sheets. *Colloids Surf., B* **2014**, *113* (0), 115−124.
(16) Perreault, F.; Tousley, M. E.; Elimelech, M. Thin-Film Composite Polyamide Membranes Functionalized with Biocidal Graphene Oxide Nanosheets. *Environ. Sci. Technol. Lett.* **2013**, *1* (1), 71−76.
(17) Geim, A. K.; Novoselov, K. S. The Rise of Graphene. *Nat. Mater.* **2007**, *6* (3), 183−191.
(18) Ruiz, O. N.; Fernando, K. A.; Wang, B.; Brown, N. A.; Luo, P. G.; McNamara, N. D.; Vangsness, M.; Sun, Y.-P.; Bunker, C. E. Graphene Oxide: a Nonspecific Enhancer of Cellular Growth. *ACS Nano* **2011**, *5* (10), 8100−8107.
(19) Dreyer, D. R.; Park, S.; Bielawski, C. W.; Ruoff, R. S. The Chemistry of Graphene Oxide. *Chem. Soc. Rev.* **2010**, *39* (1), 228−240.
(20) Das, M. R.; Sarma, R. K.; Saikia, R.; Kale, V. S.; Shelke, M. V.; Sengupta, P. Synthesis of Silver Nanoparticles in an Aqueous Suspension of Graphene Oxide Sheets and its Antimicrobial Activity. *Colloids Surf., B* **2010**, *1*, 16−22.
(21) Bao, Q.; Zhang, D.; Qi, P. Synthesis and Characterization of Silver Nanoparticle and Graphene Oxide Nanosheet Composites as a Bactericidal Agent for Water Disinfection. *J. Colloid Interface Sci.* **2011**, *360* (2), 463−470.

DOI: 10.1021/acsami.5b01639
ACS Appl. Mater. Interfaces 2015, 7, 12751−12759

(22) Faria, A. F.; Martinez, D. S. T.; Moraes, A. C. M.; Maia da Costa, M. E. H.; Barros, E. B.; Souza Filho, A. G.; Paula, A. J.; Alves, O. L. Unveiling the Role of Oxidation Debris on the Surface Chemistry of Graphene Through the Anchoring of Ag Nanoparticles. *Chem. Mater.* **2012**, *24* (21), 4080−4087.
(23) Tang, J.; Chen, Q.; Xu, L.; Zhang, S.; Feng, L.; Cheng, L.; Xu, H.; Liu, Z.; Peng, R. Graphene Oxide−Silver Nanocomposite as a Highly Effective Antibacterial Agent with Species-Specific Mechanisms. *ACS Appl. Mater. Interfaces* **2013**, *5* (9), 3867−3874.
(24) Müller, K.; Quinn, J. F.; Johnston, A. P. R.; Becker, M.; Greiner, A.; Caruso, F. Polyelectrolyte Functionalization of Electrospun Fibers. *Chem. Mater.* **2006**, *18* (9), 2397−2403.
(25) Schiffman, J. D.; Wang, Y.; Giannelis, E. P.; Elimelech, M. Biocidal Activity of Plasma Modified Electrospun Polysulfone Mats Functionalized with Polyethyleneimine-Capped Silver Nanoparticles. *Langmuir* **2011**, *27* (21), 13159−13164.
(26) Ye, P.; Xu, Z.-K.; Wu, J.; Innocent, C.; Seta, P. Nanofibrous Membranes Containing Reactive Groups: Electrospinning from Poly(acrylonitrile-co-maleic acid) for Lipase Immobilization. *Macromolecules* **2005**, *39* (3), 1041−1045.
(27) Mauter, M. S.; Wang, Y.; Okemgbo, K. C.; Osuji, C. O.; Giannelis, E. P.; Elimelech, M. Antifouling Ultrafiltration Membranes via Post-Fabrication Grafting of Biocidal Nanomaterials. *ACS Appl. Mater. Interfaces* **2011**, *3* (8), 2861−2868.
(28) Hummers, W. S.; Offman, R. E. Preparation of Graphitic Oxide. *J. Am. Chem. Soc.* **1958**, *80* (6), 1339.
(29) Tung, V. C.; Allen, M. J.; Yang, Y.; Kaner, R. B. High-Throughput Solution Processing of Large-Scale Graphene. *Nat. Nanotechnol* **2009**, *4* (1), 25−29.
(30) Tiraferri, A.; Vecitis, C. D.; Elimelech, M. Covalent Binding of Single-Walled Carbon Nanotubes to Polyamide Membranes for Antimicrobial Surface Properties. *ACS Appl. Mater. Interfaces* **2011**, *3* (8), 2869−2877.
(31) Li, J.; Liu, C.-y. Ag/Graphene Heterostructures: Synthesis, Characterization and Optical Properties. *Eur. J. Inorg. Chem.* **2010**, *2010* (8), 1244−1248.
(32) Xu, C.; Wang, X. Fabrication of Flexible Metal-Nanoparticle Films using Graphene Oxide Sheets as Substrates. *Small* **2009**, *5* (19), 2212−2217.
(33) Soldano, C.; Mahmood, A.; Dujardin, E. Production, Properties and Potential of Graphene. *Carbon* **2010**, *48*, 2127−2150.
(34) Tien, H.-W.; Huang, Y.-L.; Yang, S.-Y.; Wang, J.-Y.; Ma, C.-C. M. The Production of Graphene Nanosheets Decorated with Silver Nanoparticles for Use in Transparent, Conductive Films. *Carbon* **2011**, *49* (5), 1550−1560.
(35) Orth, E. S.; Fonsaca, J. E. S.; Domingues, S. H.; Mehl, H.; Oliveira, M. M.; Zarbin, A. J. G. Targeted Thiolation of Graphene Oxide and its Utilization as Precursor for Graphene/Silver Nanoparticles Composites. *Carbon* **2013**, *61* (0), 543−550.
(36) Rourke, J. P.; Pandey, P. A.; Moore, J. J.; Bates, M.; Kinloch, I. A.; Young, R. J.; Wilson, N. R. The Real Graphene Oxide Revelead: Stripping the Oxidative Debris from the Graphene-Like Sheets. *Angew. Chem.* **2011**, *50*, 3173−3177.
(37) Pasricha, R.; Gupta, S.; Srivastava, A. A Facile and Novel Synthesis of Ag-Graphene-Based Nanocomposites. *Small* **2009**, *20*, 2253−2259.
(38) Zhou, X.; Huang, X.; Qi, X.; Wu, S.; Xue, C.; Boey, F. Y. C.; Yan, Q.; Chen, P.; Zhang, H. In Situ Synthesis of Metal Nanoparticles on Single-Layer Graphene Oxide and Reduced Graphene Oxide Surfaces. *J. Phys. Chem. C* **2009**, *113* (25), 10842−10846.
(39) Caballero-George, C. Critical Evaluation of Biodegradable Polymers Used in Nanodrugs. *Int. J. Nanomed.* **2013**, *8*, 3071−3090.
(40) Ulery, B. D.; Nair, L. S.; Laurencin, C. T. Biomedical Applications of Biodegradable Polymers. *J. Polym. Sci., Part B: Polym. Phys.* **2011**, *49* (12), 832−864.
(41) Duan, B.; Yuan, X.; Zhu, Y.; Zhang, Y.; Li, X.; Zhang, Y.; Yao, K. A Nanofibrous Composite Membrane of PLGA−Chitosan/PVA Prepared by Electrospinning. *Eur. Polym. J.* **2006**, *42* (9), 2013−2022.
(42) Liu, S.-J.; Kau, Y.-C.; Chou, C.-Y.; Chen, J.-K.; Wu, R.-C.; Yeh, W.-L. Electrospun PLGA/Collagen Nanofibrous Membrane as Early-Stage Wound Dressing. *J. Membr. Sci.* **2010**, *355* (1−2), 53−59.
(43) Meng, Z. X.; Zheng, W.; Li, L.; Zheng, Y. F. Fabrication, Characterization and In Vitro Drug Release Behavior of Electrospun PLGA/Chitosan Nanofibrous Scaffold. *Mater. Chem. Phys.* **2011**, *125* (3), 606−611.
(44) Burger, C.; Hsiao, B. S.; Chu, B. Nanofibrous Materials and their Applications. *Annu. Rev. Mater. Res.* **2006**, *36* (1), 333−368.
(45) Jose, M. V.; Thomas, V.; Dean, D. R.; Nyairo, E. Fabrication and Characterization of Aligned Nanofibrous PLGA/Collagen Blends as Bone Tissue Scaffolds. *Polymer* **2009**, *50* (15), 3778−3785.
(46) Xu, J.; Zhang, J.; Gao, W.; Liang, H.; Wang, H.; Li, J. Preparation of Chitosan/PLA Blend Micro/Nanofibers by Electrospinning. *Mater. Lett.* **2009**, *63* (8), 658−660.
(47) Witt, M. A.; Barra, G. M. O.; Bertolino, J. R.; Pires, A. T. N. Crosslinked Chitosan/Poly (Vinyl Alcohol) Blends with Proton Conductivity Characteristic. *J. Braz. Chem. Soc.* **2010**, *21*, 1692−1698.
(48) Li, A. D.; Sun, Z. Z.; Zhou, M.; Xu, X. X.; Ma, J. Y.; Zheng, W.; Zhou, H. M.; Li, L.; Zheng, Y. F. Electrospun Chitosan-Graft-PLGA Nanofibres with Significantly Enhanced Hydrophilicity and Improved Mechanical Property. *Colloids Surf., B* **2013**, *102* (0), 674−681.
(49) Marambio-Jones, C.; Hoek, E. V. A Review of the Antibacterial Effects of Silver Nanomaterials and Potential Implications for Human Health and the Environment. *J. Nanopart. Res.* **2010**, *12* (5), 1531−1551.
(50) Liu, J.; Hurt, R. H. Ion Release Kinetics and Particle Persistence in Aqueous Nano-Silver Colloids. *Environ. Sci. Technol.* **2010**, *44* (6), 2169−2175.
(51) Sondi, I.; Salopek-Sondi, B. Silver Nanoparticles as Antimicrobial Agent: A Case Study on *E. coli* as a Model for Gram-Negative Bacteria. *J. Colloid Interface Sci.* **2004**, *275* (1), 177−182.
(52) Xu, W.-P.; Zhang, L.-C.; Li, J.-P.; Lu, Y.; Li, H.-H.; Ma, Y.-N.; Wang, W.-D.; Yu, S.-H. Facile Synthesis of Silver@Graphene Oxide Nanocomposites and their Enhanced Antibacterial Properties. *J. Mater. Chem.* **2011**, *21*, 4593−4597.
(53) Tu, Y.; Lv, M.; Xiu, P.; Huynh, T.; Zhang, M.; Castelli, M.; Liu, Z.; Huang, Q.; Fan, C.; Fang, H.; Zhou, R. Destructive Extraction of Phospholipids from *Escherichia coli* Membranes by Graphene Nanosheets. *Nat. Nanotechnol.* **2013**, *8* (8), 594−601.
(54) Akhavan, O.; Ghaderi, E. Toxicity of Graphene and Graphene Oxide Nanowalls Against Bacteria. *ACS Nano* **2010**, *4* (10), 5731−5736.
(55) Mejias Carpio, I. E.; Santos, C. M.; Wei, X.; Rodrigues, D. F. Toxicity of a Polymer-Graphene Oxide Composite Against Bacterial Planktonic Cells, Biofilms, and Mammalian Cells. *Nanoscale* **2012**, *4* (15), 4746−4756.
(56) Liu, S.; Hu, M.; Zeng, T. H.; Wu, R.; Jiang, R.; Wei, J.; Wang, L.; Kong, J.; Chen, Y. Lateral Dimension-Dependent Antibacterial Activity of Graphene Oxide Sheets. *Langmuir* **2012**, *28* (33), 12364−12372.
(57) Liu, S.; Zeng, T. H.; Hofman, M.; Burcombe, E.; Wei, J.; Jiang, R.; Kong, J.; Chen, Y. Antibacterial Activity of Graphite, Graphene Oxide, and Reduced Graphene Oxide: Membrane and Oxidative Stress. *ACS Nano* **2011**, *5* (9), 6971−6980.
(58) Hu, W.; Peng, C.; Luo, W.; Lv, M.; Li, X.; Li, D.; Huang, Q.; Fan, C. Graphene-Based Antibacterial Paper. *ACS Nano* **2010**, *4* (7), 4317−4323.
(59) Gurunathan, S.; Han, J. W.; Dayem, A. A.; Eppakayala, V.; Kim, J.-H. Oxidative Stress-Mediated Antibacterial Activity of Graphene Oxide and Reduced Graphene Oxide in *Pseudomonas aeruginosa*. *Int. J. Nanomed.* **2012**, *7*, 5901−5914.
(60) Krishnamoorthy, K.; Veerapandian, M.; Zhang, L.-H.; Yun, K.; Kim, S. J. Antibacterial Efficiency of Graphene Nanosheets against Pathogenic Bacteria via Lipid Peroxidation. *J. Phys. Chem. C* **2012**, *116* (32), 17280−17287.

DOI: 10.1021/acsami.5b01639
ACS Appl. Mater. Interfaces 2015, 7, 12751−12759